

Experimental Long-Distance Decoy-State Quantum Key Distribution Based On Polarization Encoding

Cheng-Zhi Peng,¹ Jun Zhang,² Dong Yang,¹ Wei-Bo Gao,² Huai-Xin Ma,^{1,3}
Hao Yin,³ He-Ping Zeng,⁴ Tao Yang,² Xiang-Bin Wang,¹ and Jian-Wei Pan^{1,2,5}

¹*Department of Physics, Tsinghua University, Beijing 100084, China*

²*Hefei National Laboratory for Physical Sciences at Microscale and Department of Modern Physics, University of Science and Technology of China, Hefei, Anhui 230026, China*

³*China Electronics System Engineering Company, Beijing 100039, China*

⁴*Key Laboratory of Optical and Magnetic Resonance Spectroscopy and Department of Physics, East China Normal University, Shanghai 200062, China*

⁵*Physikalisches Institut, Universität Heidelberg, Philosophenweg 12, 69120 Heidelberg, Germany*

(Dated: January 1, 2019)

We demonstrate the decoy-state quantum key distribution (QKD) with one-way quantum communication in polarization space over 102 km. Further, we simplify the experimental setup and use only one detector to implement the one-way decoy-state QKD over 75 km, with the advantage to overcome the security loopholes due to the efficiency mismatch of detectors. Our experimental implementation can really offer the unconditionally secure final keys. We use 3 different intensities of 0, 0.2 and 0.6 for the pulses of source in our experiment. In order to eliminate the influences of polarization mode dispersion in the long-distance single-mode optical fiber, an automatic polarization compensation system is utilized to implement the active compensation.

PACS numbers: 03.67.Dd, 42.81.Gs, 03.67.Hk

Quantum key distribution [1, 2, 3] can in principle offer the unconditional secure private communications between two remote parties, Alice and Bob. However, the security proofs for the ideal BB84 protocol [4, 5] do not guarantee the security of a specific set-up in practice due to various imperfections there. One important problem in practical QKD is the effects of the imperfect source, say, the coherent states. The decoy state method [6, 7, 8, 9, 10] or some other methods [11, 12] can help to generate the unconditional final keys even an imperfect source is used by Alice in practical QKD. Basically, QKD can be realized in both free space and optical fiber [2]. Each option has its own advantages. The fiber QKD can be run in the always-on mode: it runs in both day and night and is not affected by the weather. Also, the future local QKD networks are supposed to be using fiber. So far, there are many experiments of fiber QKD with weak coherent lights [13]. However, these results actually do not offer the unconditional security because of the possible photon-number-splitting attack [14]. Recently, there are also experimental implementations with the decoy-state method for a distance of 13 km and 60 km respectively [15], with two-way quantum communication. However, since these implementations have not taken the specific operations as requested by Ref. [16], the security of the final keys is still unclear due to the so-called Trojan horse attacks [2]. One can implement active counter-measures [16] to overcome this problem, which is deserved experimental implementations in the future. The other way is to use one-way quantum communication which we have adopted in this work.

Here we present the first polarization-based decoy-

state QKD implementation over 102 km with only one-way quantum communication using two detectors and 75 km using only one detector. Our results are unconditionally secure (For the unconditional security, we mean that the probability that Eve has non-negligible amount of information about the final key is exponentially close to 0, say, $e^{-O(100)}$). Here we must clarify that given the existing technologies [13], if the distance is shorter than about 20 km, through the simple worst-case estimation [18] of the fraction of tagged bits it is still possible for one to implement the unconditionally secure QKD without using the decoy-state method.

We can know how to distill the secure final keys with imperfect source given the separate theoretical results from Ref. [18], if we know the upper bound of the fraction of tagged bits (those raw bits generated by multi-photon pulses from Alice) or equivalently, the lower bound of the fraction of untagged bits (those raw bits generated by single-photon pulses from Alice). In Wang's 3-intensity decoy-state theory [7, 8], one can randomly use 3 different intensities (average photon numbers) of each pulses (0, μ , μ') in the protocol and then observe the counting rates of pulses of each intensities, say $S_0, S_\mu, S_{\mu'}$. The density operators for states of intensity μ and μ' ($\mu' > \mu$) are

$$\begin{cases} \rho_\mu = e^{-\mu}|0\rangle\langle 0| + \mu e^{-\mu}|1\rangle\langle 1| + c\rho_c \\ \rho_{\mu'} = e^{-\mu'}|0\rangle\langle 0| + \mu' e^{-\mu'}|1\rangle\langle 1| + \frac{\mu'^2 e^{-\mu'}}{\mu^2 e^{-\mu}} c\rho_c + d\rho_d, \end{cases} \quad (1)$$

here $c = 1 - e^{-\mu} - \mu e^{-\mu}$, $\rho_c = \frac{e^{-\mu}}{c} \sum_{n=2}^{\infty} \frac{\mu^n}{n!} |n\rangle\langle n|$ and $d > 0$. We denote $s_0(s'_0), s_1(s'_1), s_c(s'_c)$ for the counting rates of those vacuum pulses, single-photon pulses and ρ_c pulses from $\rho_\mu(\rho_{\mu'})$. Asymptotically, the values of primed symbols here should be equal to those values

of unprimed symbols. However, in an experiment the number of samples is finite therefore they could be a bit different. The bound values of s_1, s'_1 can be determined by the following joint constraints

$$\begin{cases} S_\mu = e^{-\mu}s_0 + \mu e^{-\mu}s_1 + cs_c \\ cs'_c \leq \frac{\mu'^2 e^{-\mu'}}{\mu'^2 e^{-\mu'}}(S_{\mu'} - \mu' e^{-\mu'}s'_1 - e^{-\mu'}s'_0), \end{cases} \quad (2)$$

where $s'_1 = (1 - \frac{10e^{\mu/2}}{\sqrt{\mu s_1 N_\mu}})s_1$, $s'_c = (1 - \frac{10}{\sqrt{s_c N_\mu}})s_c$, $s'_0 = 0$ and $s_0 = (1 + r_0)S_0 = (1 + \frac{10}{\sqrt{S_0 N_0}})S_0$ to obtain the worst-case results [7, 8] and N_μ, N_0 are the pulse numbers of intensity $\mu, 0$ respectively. Given these, one can calculate s_1, s'_1, s_c numerically.

The experimental setup is shown in Fig.1, mainly including transmitter (Alice), quantum channel, receiver (Bob) and electronics system. All the electronics modules are designed by ourselves. The synchrodyne (SD) is designed by field programmable gate array (FPGA, Altera Co.) and outputs multiple channels of synchronous clocks with independent programmable parameter settings, which is equivalent to an arbitrary function generator, to drive the modules of random number generator (RNG), data acquisition (DAQ, designed by FPGA) and single-photon detector (SPD) respectively. Then the signals with the FWHM of about 1 ns are generated by laser diode driver (LDD) to drive 10 DFB laser diodes (LD) at the central wavelength of 1550 nm, where 4 LDs are used for decoy states (μ) and another 4 LDs are used for signal states (μ') and the other 2 LDs are used for polarization calibration. The polarization states of photons emitting from LDs can be transformed to arbitrary polarization state by polarization controller (PC). For decoy states and signal states, the four polarization states are $|H\rangle, |V\rangle, |+\rangle, |-\rangle$, where $|H\rangle, |V\rangle$ represent horizontal polarization and vertical polarization, $|+\rangle = 1/\sqrt{2}(|H\rangle + |V\rangle)$ and $|-\rangle = 1/\sqrt{2}(|H\rangle - |V\rangle)$, as the four states for the standard BB84 protocol [1]. For test states, the two polarization states are $|H\rangle$ and $|+\rangle$ to calibrate the two sets of polarization basis in Bob's side. Further the photons of every channel are coupled to an optical fiber via fiber coupling network (FCN), which is composed of multiple beam splitters (BS) and polarization beam splitters (PBS) and optical attenuators. In FCN, the fiber length of every channel must be adjusted precisely so that the arrival time differences to SPD caused by the fiber length differences can be less than 100 ps.

However, the central wavelengths of every LD have very slight variance. In the experiment, we insert a DWDM fiber filter (FF) in Alice's side. On the one hand, it can guarantee that the wavelengths of emitted photons in all channels are same to avoid the possibility of Eve's attack utilizing the variance of photon wavelengths. On the other hand, it can reduce the influences of chromatic dispersion in long-distance fiber.

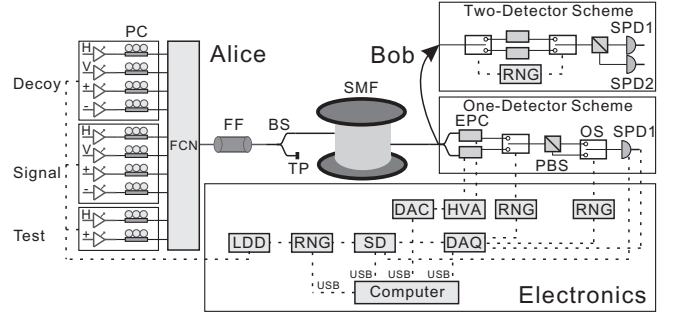


FIG. 1: Schematic diagram of the experimental setup. Solid line and dashed line represent optical fiber and electric cable respectively. PC, polarization controller; FCN, fiber coupling network; FF, fiber filter; BS, beam splitter; TP, test point; SMF, single-mode fiber; DL, delay line; EPC, electric polarization controller; PBS, polarization beam splitter; OS, optical switch; SPD, single-photon detector; LDD, laser diode driver; RNG, random number generator; SD, synchrodyne; DAC, digital-to-analog converter; HVA, high voltage amplifier; DAQ, data acquisition; USB, universal serial bus.

In Wang's decoy-state protocol [7, 8], 3 different intensities of weak coherent light, i.e., signal states and decoy states and vacuum are used. According to the simulation of experimental parameters, the pulse numbers ratio of these 3 intensities is 5 : 4 : 1. And the intensities of signal states and decoy states are fixed at $\mu' = 0.6$ and $\mu = 0.2$ respectively. The fluctuations of the intensities are monitored at the test point (TP).

After passing through the long-distance single-mode fiber (SMF, Corning Co.), at Bob's side we adopt two kinds of measurement scheme. In one-detector scheme, firstly a fiber BS is used to select the two polarization measurement basis called HV basis and $+-$ basis randomly. Secondly due to the polarization mode dispersion (PMD) effects in long-distance SMF, we develop an automatic polarization compensation (APC) system to compensate for the PMD actively. The principles of APC are: Alice sends fixed $|H\rangle$ states or $|+\rangle$ states. Then Bob records the accepted counting rates in the corresponding basis using DAQ system and transmits them to the computer via universal serial bus (USB). After algorithmic processing, the computer gives out the data, which can be converted to voltages of electric polarization controllers (EPC, General Photonics Co.) through digital-to-analog converter (DAC) and high voltage amplifier (HVA). Then the fiber squeezers in EPC are driven by the voltages and change the polarization [19]. After repeating feedback controls the visibility of test states at Bob's side can reach the target value and the APC system stops. When the visibility is degraded to below the threshold value the APC system will restart. The average adjusting time is about 3 minutes. Figure 2(a) shows the test results of the APC system in the case of 75 km optical fiber. Thirdly we use two magnetic optical

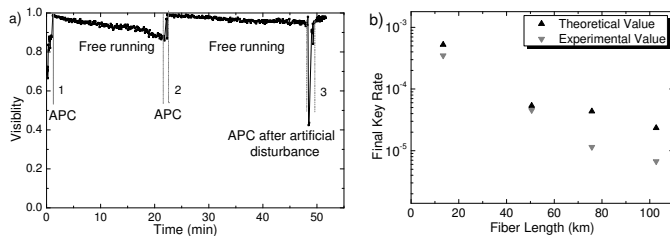


FIG. 2: a) Test of the automatic polarization compensation (APC) system with 75 km optical fiber. In position 1 and 2 the APC system monitors the visibility changes of polarization states and adjusts the voltages of EPC actively to reach the target visibility. Subsequently, the visibility of polarization states become worse slowly when free running. In position 3, artificial disturbance induces the drastic change of visibility and the APC system can still work well. b) Comparison of the final key generation rate of signal states per pulse between the theoretical calculation and experimental results with different distance settings. The four fiber lengths are 13.448 km, 50.524 km, 75.774 km and 102.714 km. The first three settings use one-detector scheme and the last one uses two-detector scheme. The first two settings' repetition frequency is $f=4$ MHz and the last two is $f=2.5$ MHz.

switch (OS, Primanex Co.) driven by two independent RNG modules, whose switching time is less than 20 μ s to randomly switch the basis and the output ports of PBS respectively. The one-detector scheme can overcome the security loopholes due to the efficiency mismatch of detectors [17] since the fiber lengths of each state can be adjusted identically. Comparison to the one-detector scheme, two OS driven by the same RNG and two SPDs ($\eta_{D1} \approx 7\%$, $\eta_{D2} \approx 6\%$) with low dark counts are used in two-detector scheme to reduce the transmission losses in Bob's side.

We use this all-fiber quantum cryptosystem to implement the experimental demonstration of polarization-based 3-intensity decoy-state QKD over 102 km and 75 km using two-detector scheme and one-detector scheme respectively. The experimental parameters and their corresponding values are listed in Table I. In the experiment, Alice totally transmits about N pulses to Bob. After the transmission Bob announces the pulse sequence numbers and basis information of received states. Then Alice broadcasts to Bob the actual state information (decoy states or signal states or vacuum) and basis information of the corresponding pulses. Then Alice and Bob can calculate the parameters of $S_{\mu'}$, S_{μ} , S_0 , $E_{\mu'}$ and E_{μ} , where $E_{\mu'}$ and E_{μ} are the experimental observed quantum bit error rate (QBER) values of signal states and decoy states respectively.

Further, we can numerically calculate a tight lower bound of the counting rate of single-photon using the Eqs. 2. The calculation result, s'_1 , is shown in Table I. The next step is to estimate the fraction of single-photon Δ_1 and the QBER upper bound of single-photon E_1 . In

TABLE I: Experimental parameters and their corresponding values of 75.774 km (Value1) and 102.714 km (Value2) decoy-state QKD.

Para.	Value1	Value2	Para.	Value1	Value2
$length$	75.774	102.714	$S_{\mu'}$	2.076×10^{-4}	1.262×10^{-4}
f	2.5 M	2.5 M	S_{μ}	7.534×10^{-5}	4.611×10^{-5}
N	1.607 G	5.222 G	S_0	9.174×10^{-6}	6.711×10^{-6}
μ'	0.6	0.6	s'_1	2.460×10^{-4}	1.558×10^{-4}
μ	0.2	0.2	$R_{\mu'}$	1.143×10^{-5}	6.706×10^{-6}
$E_{\mu'}$	3.231%	3.580%	R_E	12.154 Hz	8.427 Hz
E_{μ}	9.039%	9.098%	R_T	46.167 Hz	29.427 Hz
$E_1^{\mu'}$	6.099%	5.854%	R_E/R_T	0.263	0.284

order to estimate the final key rate conservatively, we use

$$\begin{cases} \Delta_1^{\mu'} = s'_1 \mu' e^{-\mu'} / S_{\mu'} \\ \Delta_1^{\mu} = s_1 \mu e^{-\mu} / S_{\mu} \end{cases} \quad (3)$$

to calculate the fraction of single-photon in signal states and decoy states respectively [7, 8]. Then we can further estimate the QBER upper bound of single-photon in signal states and decoy states respectively, i.e.,

$$\begin{cases} E_1^{\mu'} = (E_{\mu'} - \frac{(1-r_0)S_0 e^{-\mu'}}{2S_{\mu'}}) / \Delta_1^{\mu'} \\ E_1^{\mu} = (E_{\mu} - \frac{(1-r_0)S_0 e^{-\mu}}{2S_{\mu}}) / \Delta_1^{\mu}. \end{cases} \quad (4)$$

Here we consider the statistical fluctuations of the vacuum states to obtain the worst-case results.

Lastly we can calculate the final key rates of signal states and decoy states using the formula [7, 8] of

$$\begin{cases} R_{\mu'} = S_{\mu'} (\Delta_1^{\mu'} - H(E_{\mu'}) - \Delta_1^{\mu'} H(E_1^{\mu'})) \\ R_{\mu} = S_{\mu} (\Delta_1^{\mu} - H(E_{\mu}) - \Delta_1^{\mu} H(E_1^{\mu})). \end{cases} \quad (5)$$

The final key rate of signal states in our experiment is $R_E = (5/10)fR_{\mu'}$. Then We compare our results with the theoretically allowed value R_T , i.e., in the case both Δ_1 and E_1 are known without any overestimation. The theoretically allowed best values of Δ_1 and E_1 for signal states are

$$\begin{cases} \Delta_{1T}^{\mu'} = (S_{\mu'} - (1 - \mu')S_0)e^{-\mu'} / S_{\mu'} \\ E_{1T}^{\mu'} = (E_{\mu'} - \frac{S_0 e^{-\mu'}}{2S_{\mu'}}) / \Delta_{1T}^{\mu'}, \end{cases} \quad (6)$$

with the assumption that the ideal value of the single-photon counting rate $s_{1T} = \eta + S_0$ and $S_{\mu'} = \eta\mu' + S_0$, where η is the overall transmittance including the detection efficiency of the SPD. We find out that our experimental results in the two cases are both close to 30% of the theoretically allowed maximum value.

In our experiment, the raw bits caused by those decoy pulses can also be used to generate the final keys. During the above calculation, we have used the worst-case results

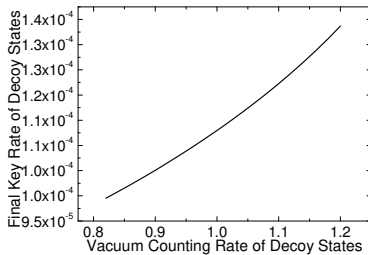


FIG. 3: The final key rate of decoy pulses varies with the vacuum counting rate of s_0 in the case of 13.448 km. The unit of horizontal axis is S_0 (the observed counting rate of those vacuum pulses in the experiment).

in every step for the security. Obviously, there are more economic methods for the calculation of final key rate. Consider the key rate calculation of decoy states above. In calculating Δ_1^μ , we assumed the worst case of $s_0 = (1+r_0)S_0$, while in estimating the QBER of single-photon pulses E_1^μ , we assumed the worst case of $s_0 = (1-r_0)S_0$. Although we don't exactly know the true value of s_0 , there must be one fixed value for both calculations of Δ_1^μ and E_1^μ . Therefore we can also safely calculate the final key rate in the following way: choose one possible value of s_0 , use this value to calculate both Δ_1^μ and $E_1^\mu = (E_\mu - \frac{s_0 e^{-\mu}}{2S_\mu})/\Delta_1^\mu$ and then calculate the possible key rate. We try all possible values of $(1-r_0)S_0 \leq s_0 \leq (1+r_0)S_0$ and then pick out the smallest value as the lower bound of decoy states key rate. Figure 3 demonstrates the results with all possible values of s_0 in the case of 13.448 km. We find that the smallest value there is still larger than the experimental final key rate of the decoy pulses.

Also, we have tested the system with different fiber lengths and compared the final key rates with the theoretically allowed maximum values, see Fig.2(b). The differences between the experimental values and the theoretical values are mainly due to the imperfect polarization compensation and the possible statistical fluctuation.

The one-detector scheme and two-detector scheme each have their own advantages. One-detector scheme can overcome the time-shift attack and generate the unconditionally secure final keys while the latter can implement longer distance. If we use four high quality detector with the same parameters the final key rate and maximum distance will be improved. Also, the balance between the efficiency and the dark counts is important. During the experiment, we have even reduced the efficiency of the SPD purposely to reduce the dark counts to obtain better balance. Hopefully, a low-noise and high-efficiency detector at telecommunication wavelengths can be used in the future to further improve the final key rate. The superconducting transition-edge sensor is one of the promising candidates in the future [20].

In summary, we implement the polarization-based one-way decoy-state QKD over 102 km. Moreover, we also implement 75 km one-way decoy-state QKD using only

one detector. Our experiment can really offer the unconditionally secure final keys.

This work is supported by the NNSF of China, the CAS and the National Fundamental Research Program.

-
- [1] C.H. Bennett and G. Brassard, in *Proc. of IEEE Int. Conf. on Computers, Systems, and Signal Processing (IEEE, New York, 1984)*, pp. 175-179.
 - [2] N. Gisin, G. Ribordy, W. Tittel, and H. Zbinden, *Rev. Mod. Phys.* **74**, 145 (2002).
 - [3] M. Dusek, N. Lütkenhaus, M. Hendrych, in *Progress in Optics VVVX*, edited by E. Wolf (Elsevier, 2006).
 - [4] D. Mayers, *J. ACM* **48**, 351 (2001); Its preliminary version appeared in *Advances in Cryptology-Proc. Crypto96* Vol.1109 of *Lecture Notes in Computer Science*, edited by N. Kobitz.
 - [5] P. W. Shor and J. Preskill, *Phys. Rev. Lett.* **85**, 441 (2000).
 - [6] W.-Y. Hwang, *Phys. Rev. Lett.* **91**, 057901 (2003).
 - [7] X.-B. Wang, *Phys. Rev. Lett.* **94**, 230503 (2005).
 - [8] X.-B. Wang, *Phys. Rev. A* **72**, 012322 (2005).
 - [9] H.-K. Lo, X. Ma, and K. Chen, *Phys. Rev. Lett.* **94**, 230504 (2005); X. Ma *et al.*, *Phys. Rev. A* **72**, 012326 (2005).
 - [10] J.W. Harrington *et al.*, quant-ph/0503002.
 - [11] V. Scarani, A. Acin, G. Robordy, N. Gisin, *Phys. Rev. Lett.* **92**, 057901 (2004); C. Branciard, N. Gisin, B. Kraus, V. Scarani, *Phys. Rev. A* **72**, 032301 (2005).
 - [12] M. Koashi, *Phys. Rev. Lett.* **93**, 120501(2004); K. Tamaki, N. Lütkenhaus, M. Loashi, J. Batuwantudawe, quant-ph/0607082.
 - [13] M. Bourennane *et al.*, *Opt. Express* **4**, 383 (1999); D. Stucki *et al.*, *New J. Physics*, **4**, 41, (2002); H. Kosaka *et al.*, *Electron. Lett.* **39**, 1199 (2003); C. Gobby, Z.L. Yuan, and A.J. Shields, *Appl. Phys. Lett.* **84**, 3762 (2004); X.-F Mo *et al.*, *Opt. Lett.* **30**, 2632 (2005).
 - [14] B. Huttner *et al.*, *Phys. Rev. A* **51**, 1863 (1995); H.P. Yuen, *Quantum Semiclassic. Opt.* **8**, 939 (1996); G. Brassard *et al.*, *Phys. Rev. Lett.* **85**, 1330 (2000); N. Lütkenhaus, *Phys. Rev. A* **61**, 052304 (2000); N. Lütkenhaus and M. Jähma, *New J. Phys.* **4**, 44 (2002).
 - [15] Y. Zhao *et al.*, *Phys. Rev. Lett.* **96**, 070502 (2006); Y. Zhao *et al.*, quant-ph/0601168.
 - [16] N. Gisin *et al.*, *Phys. Rev. A* **73**, 022320 (2006).
 - [17] V. Makarov *et al.*, quant-ph/0511032; B. Qi *et al.*, quant-ph/0512080.
 - [18] H. Inamori, N. Lütkenhaus, D. Mayers, quant-ph/0107017; D. Gottesman, H.K. Lo, N. Lütkenhaus, and J. Preskill, *Quantum Inf. Comput.* **4**, 325 (2004).
 - [19] R. Noé, *Electron. Lett.* **22**, 772-773 (1986); N. G. Walker and G. R. Walker, *Electron. Lett.* **23**, 290-292 (1987); R. Noé, H. Heidrich, and D. Hoffmann, *J. Lightwave Technol.* **6**, 1199-1207 (1988).
 - [20] K.D. Irwin, *Appl. Phys. Lett.* **66**, 1998 (1995); B. Cabrera *et al.*, *Appl. Phys. Lett.* **73**, 735 (1998); D. Rosenberg *et al.*, *Phys. Rev. A* **71**, 061803(R) (2005).